Numerical Study of Optimum Configuration of Unconventional Airfoil with Steps and Rotating Cylinder for Best Aerodynamics Performance

Dr. Najdat N. Abdulla
Professor
College of Engineering-University of Baghdad
Najdat_abdulla@yahoo.co.uk

Ahmed J. Hamoud
M.sc.
College of Engineering-University of Baghdad
ahmed_alzaidy80@yahoo.com

ABSTRACT

Numerical study of separation control on symmetrical airfoil, four digits (NACA 0012) by using rotating cylinder with double steps on its upper surface based on the computation of Reynolds-average Navier- Stokes equations was carried out to find the optimum configuration of unconventional airfoil for best aerodynamics performance. A model based on collocated Finite Volume Method was developed to solve the governing equations on a body-fitted coordinate system. A revised (k-w) model was proposed as a known turbulence model. This model was adapted to simulate the control effects of rotating cylinder. Numerical solutions were performed for flow around unconventional airfoil with cylinder to main stream velocities ratio in the range of 1 to 4 and for various positions of the steps on the airfoil from the leading edge, 0.1c, 0.2c, 0.3c, 0.4c, 0.5c for the first step and 0.5c, 0.6c, 0.7c, 0.8c for the second step with constant step depth and length of 0.03c and 0.125c respectively. Reynolds number of 700,000 which was based on the cord length (c), with angle of attacks 0, 5, 8, 10, 12, 15 degrees was considered for the assessment of the unconventional airfoil performance. The numerical investigation showed that the optimum configuration for the unconventional airfoil was found to be at velocities ratio ($U/U\infty=4$) with the steps positions at 0.5c and 0.8c for best airfoil performance.

Keywords: unconventional airfoil, airfoil with rotating cylinder, airfoil with upper steps.

دراسة عددية للشكل الامثل لجناح غير تقليدي يحوي على عتبات واسطوانة دوارة لأفضل اداء ديناميكي هوائي

د.نجدت نشأت عبدالله
استاذ
كلية الهندسة- جامعة بغداد

احمد جميل حمود
ماجستير
كلية الهندسة- جامعة بغداد

الخلاصة

باستخدام (NACA 0012)تضمن العمل دراسة عددية للسيطرة على انفصال جريان الهواء من على سطح جناح متناظر نوع اسطوانة دوارة في مقدمة الجناح واضافة عتبات اثنين على السطح العلوي للجناح, وهذا التحليل تم باستخدام معادلة متوسط رينولد- نافير ستوك) وذلك لايجاد افضل اداء ايروديناميكي للجناح بعد الاضافات. اعتمد هذا الموديل الرياضي على طريقة الحجوم المحددة لحل , وقد تم استخدام موديل رياضي للجريان الاضطرابي. أجري الحل العددي للتدفق حول الجناح غير التقليدية مع اسطوانة دوارة بنسبة السرعات من 1 الى 4 اضعاف سرعة التيار الهوائي الرئيسي ومع اختلاف اماكن العتبات على الجناح بمسافة مقاسة من الحافة الأمامية وقد كان عدد رينولدز من 700.000 مع زاوية من الهجمات 0، 5، 8، 10، 12، 15 درجة لتقييم الأداء الجناح غير تقليدية.

1. INTRODUCTION

In modern civil transport aircraft, the main objectives to be achieved are the needs of cruise conditions (low drag) with a particular attention on the economic, as well as aerodynamic efficiency because most of the flight time is spent during this phase of flight at transonic conditions. Hence, the shape of the wing must be able to minimize the strength of any shock waves present in order to reduce the wave drag. In addition, the wing must be able to satisfy the necessary requirements of take-off and landing. Therefore, complementary high-lift systems are usually employed by combat aircraft, not only for short take-off and landing, but also to enhance high-speed maneuverability by delaying the onset of high-speed stall. High-lift system mainly consists of mobile mechanical device capable of separating some parts of the wing and repositioning them in a suitable configuration in order to increase the chamber and effective area of the wing. The result of these arrangements is a new configuration, which allows a significant improvement in lifting capabilities compared to the clean wing of the cruise configuration. The first practical application of the moving surface for the boundary layer control was demonstrated by, **Favre, 1938**. He studied an airfoil with an upper surface formed by a belt moving over two rollers. The separation was delayed until the angle of attack reached to 55 degree, where the maximum lift coefficient of 3.5 was realized. **Cichy, et al., 1972**, studied the application of rotating cylinder to improve ship maneuverability. Extension force measurements and flow visualization experiments were conducted using a large circulating water channel. Three different configurations of rudder were used with the rotating cylinder; (1) in insulation, (2) the leading-edge of the rudder, and (3) combined with a flap-rudder where the cylinder being at the leading-edge of the flap. From the overall consideration of hydrodynamic performance and mechanical complexity, configuration number (2) was preferred as far as power consumption concerned. **Buckholtz, 1986**, observed the irregular shape of many insect wings as well as other studies indicating a higher lift on these wings. A flow visualization scheme was used to observe and photograph stream lines around two different wing sections. One of these, a sheet metal model with geometry matching that of a butterfly wing, was studied at a Reynolds number of 1500 and 80 based on corrugation depth. **Freymuth,et al, 1989**, worked on the airfoil with rotating cylinder at the nose to demonstrate concept of dynamic separation without dynamic stall. The airfoil was tested in the wind tunnel with uniform velocity of 61 cm/s and cylinder rotating speed of 3000 r.p.m. at a Re=4300 based on the chord length. They found that for a pitch angle of 20^o a speed ratio was 2.5, for 40^o the ratio was 4.2, and at 90^o it was 12. An increase in speed ratio beyond the minimum had no detrimental effect on stall control but resulted in a wall jet passing over the suction side of the airfoil which continued as a jet behind the trailing edge. These results were inferred from flow visualization and confirmed by speed profiles obtained with a hot-wire anemometer, after the final pitch position of the airfoil had been reached. **Al- Tornachi, and Abu- Tabikh, 1998**, developed a numerical method to analyze steady incompressible flow around airfoils with turbulent separation. The model used was a direct viscous- inviscid interaction scheme based on a vortex panel method. The overall method was relatively simple and allowed for predicting the complete wing characteristics. Some example calculations were discussed, and good agreement between calculations and experiment was obtained. **Al-Garni, et al., 2000**, worked on the experimental investigation of two –dimensional NACA 0024 airfoil equipped with a leading-edge rotating cylinder. The airfoil was stated for different angles, and they found that the leading-edge rotating cylinder increases the lift coefficient of a NACA 0024 airfoil from 0.85 at Uc/U=0 to 1.63 at Uc/U=4 and delay the stall angle of attack by about 160%. In the same year, Yeung, 2000, studied

the flow visualization on a corrugated airfoil. He confirmed that the trapped vortices leaded to a modification of the effective wing shape and an increase in lift. He also, found that the leading-edge rotating cylinder effectively extend the lift curve of an airfoil without substantially affecting its slop. **Sahu, and Patnaik, 2010**, investigated the flow past NACA 0012 airfoil. The simulations were performed for different angles of attack varying from 0^o to 20^o in sub- critical Reynolds numbers range. The results observed that, stall occurred at $\alpha=12^o$ and Re=46400.Also, the stall angle was delayed by using the simple momentum injection technique with the help of one rotating element as an actuator disc on the leading edge of airfoil. **Lukas, et al., 2011**, studied the boundary layer separation, both stall and separation bubbles, related to the low-Reynolds number transition mechanism. Airfoil of three czech-designed sailplanes and their wing-fuselage interaction were subjected to study. Effect of passive flow control device-vortex generators was surveyed and counter- rotating vortex generators was applied. Separation suppression was reached and consequent drag coefficient reduction of test aircrafts was measured in flight. All above studies were neither considered the combine effects of leading edge rotating cylinder and the steps on the upper side of airfoil nor high Reynolds numbers flow.

The present work investigate the combine effect of the rotating cylinder of diameter 0.1c in leading edge and double steps at different locations with constant depths and length on the upper side of airfoil. Symmetrical airfoil four digits, (NACA 0012) with Reynolds number of 700000 were considered in this work. Upon the numerical results of all above considered cases, an optimum configuration of airfoil which is represented by lengths, depths and positions of each step in addition to the cylinder to mainstream velocities ratio were obtained for the best performance enhancement of unconventional airfoil.

2. MATHEMATICAL FORMULATION

2.1 Governing Partial Differential Equations

In the present work, the working fluid is air and flow was considered to be steady, two dimensional mean flows, fully turbulent, incompressible, and Newtonian fluid.

The governing equations were derived in Cartesian coordinate systems. Finite volume methods for solving differential equations require continuous physical space to be discretized into a uniform computational space. However, the applications of the boundary conditions require that the boundaries of the physical space fall on coordinate lines of the coordinate system.

In order to analyze the flow field around the airfoil with rotating cylinder and two steps, solution of two dimensional Navier-Stokes equations is required, due to the complexity of flow around airfoil configurations and the dominancy of viscosity effects.

The governing equations for the mean velocity and pressure are the mass and momentum equations, these are analyzed the averaged Navier- Stokes equations. A two- equation turbulence model (k-ω) is used for the system of the momentum equations.

2.2 Reynolds-averaged Navier- Stokes Equations

The basic governing fluid flow equations for, incompressible flows will be summarized. The derivation of these equations, details regarding the constitutive relations used and the various turbulence modeling assumptions employed can be found in several references, **White, 1991,and Ferziger and Peric, 1999.**

Employing indicial notation, the instantaneous form of continuity and momentum equations in Cartesian coordinates can be written as follows:

$$\frac{\partial}{\partial x_j}(u_j) = 0 \quad (1)$$

$$\frac{\partial}{\partial x_j}(\rho u_i u_j) = -\frac{\partial P}{\partial x_i} + \frac{\partial \tau_{ij}}{\partial x_j} \quad (2)$$

Where x_i is position vector, τ_{ij} is viscous stress tensor. The constitutive relation between stress and strain rate for a Newtonian fluid is used to relate the components of the stress tensor to velocity gradients:

$$\tau_{ij} = \mu\left(\frac{\partial u_i}{\partial x_j} + \frac{\partial u_j}{\partial x_i}\right) - \frac{2}{3}\mu\frac{\partial u_i}{\partial x_j}\cdot\delta_{ij} \quad (3)$$

Where μ represents the molecular viscosity and δ_{ij} is the Kronecker delta. The conservation equations above hold exactly for laminar flows. For turbulent flows, in the context of RANS methods, ensemble averaging will be resorted. The time- averaged form of the above equations for turbulent flows is obtained by mass- averaging. The various flow properties are decomposed into mean and fluctuating components, as follows:

$$u_i = \bar{u}_i + u_i' \quad (4)$$

$$\tau_{ij} = \bar{\tau}_{ij} + \tau_{ij}' \quad (5)$$

$$P = \bar{P} + P' \quad (6)$$

Note that Favre-averaging is used for u_i and τ_{ij} (bar and prime denote a Favre- averaging mean quantity and the fluctuation above this mean, respectively). Reynolds- averaging is used for P (bar and prime denote a Reynolds- Averaged mean quantity and the fluctuation above this mean, respectively). After mass- averaging, the mean- flow governing equations become:

$$\frac{\partial}{\partial x_j}(\bar{u}_j) = 0 \quad (7)$$

$$\frac{\partial}{\partial x_j}(\rho\bar{u}_j\bar{u}_i) = -\frac{\partial \bar{P}}{\partial x_i} + \frac{\partial}{\partial x_j}(\tilde{\tau}_{ij} - \rho\overline{u_i'u_j'}) \quad (8)$$

The double correlation between u_i' and itself, which appears in the term on the right hand side of equation , is the kinetic energy per unit volume (k) of the turbulent velocity fluctuations and can be defined as:

$$k = \frac{1}{2}\overline{u_i'u_j'} \quad (9)$$

The term $\rho\overline{u_i'u_j'}$ is called the Reynolds-stress tensor and can be shown by:

$$\bar{\rho}\sigma_{ij} = -\rho\overline{u_i'u_j'} \quad (10)$$

Or

$$\sigma_{ij} = -\overline{u_i'u_j'} \quad (11)$$

$$\sigma_{ij} = -\overline{u_i' u_j'} = \mu_t \left(\frac{\partial \bar{u}_i}{\partial x_j} + \frac{\partial \bar{u}_j}{\partial x_i} \right) - \frac{2}{3} \mu_t \frac{\partial \bar{u}_i}{\partial x_j} \cdot \delta_{ij} - \frac{2}{3} \rho k \cdot \delta_{ij} \quad (12)$$

Two major approaches are currently used to model these terms, namely:

(a) Eddy Viscosity Models (EVM)
(b) Reynolds- Stress Models (RSM)

The EVM employ Boussineq's eddy hypothesis, which relates the Reynolds stresses to the gradient of mean variables as follows:

Where μ_t is the turbulent (eddy) viscosity. In the most common models in this category, it is postulated that eddy viscosity is dependent on the kinetic energy of the turbulent velocity fluctuations (k) and its dissipation rate (ε) or some combination thereof (such as $\omega = \varepsilon/k$). These variables, in turn are computed by solving transport equations which employ some modeling assumption. On the other hand, the RSM, , estimate the Reynolds stresses by solving transport equations for σ_{ij}. Modeling assumption are required to close the transport equations for σ_{ij}; since the modeled terms are of a higher order than those in the EVM. The RSM are also called second-order closure or second-moment closure models. Incorporating the above modeling assumption, the governing equations for turbulent flow using EVM can be expressed as:

- Continuity equation:

$$\frac{\partial}{\partial x_j} (\bar{\rho} \bar{u}_j) = 0 \quad (13)$$

- Momentum equation:
- $$\frac{\partial}{\partial x_j} \left(\rho \bar{u}_j \bar{u}_i \right) = -\frac{\partial \bar{P}}{\partial x_i} + \frac{\partial}{\partial x_j} \left((\mu + \mu_t) \left(\frac{\partial \bar{u}_i}{\partial x_j} + \frac{\partial \bar{u}_j}{\partial x_i} \right) - \frac{2}{3} \mu_t \frac{\partial \bar{u}_i}{\partial x_j} \cdot \delta_{ij} \right) \quad (14)$$

2.3 Boundary Conditions

-Inlet boundary

At inlet, the velocity components (u and v), the static pressure, the turbulent kinetic energy (k) and its dissipation rate (ε) and ($\omega = \varepsilon/k$) are specified. The values of ($k, \varepsilon \; and \; \omega$) are approximated based on assumed turbulence intensity (Ti) typically between (1% and 6%) and length scale approximation. Approximate value of ($k, \varepsilon \; and \; \omega$) for internal flows can be obtained by means of the following simple assumed forms, **Versteeg and Malalasekera,1995**;

$$k_{in} = \frac{3}{2} (u_i . T_i)^2 \quad (15)$$

$$\varepsilon_{in} = C_\mu^{3/4} \frac{k^{3/2}}{l}, \quad l = 0.07L \quad (16)$$

Where; u_i: Inlet velocity.

T_i: Turbulence intensity.

L: Equivalent length.

C_μ : Universal constant, 0.09

l: Length scale of turbulence.

Moult, and Srivatsa, 1977, assumed that (k, ε *and* ω) are specified with (k) taken arbitrary as (3%) of the incoming specific kinetic energy and (ε) evaluated with assumed length scale (1) equals (3%) of the domain dimension.

- Outlet boundary

Usually the velocity is known only where the fluid enters the physical domain. At outlet, the velocity distribution is decided by what happens within the domain, **Moult, and Srivatsa, 1977 and Versteeg, and Malalasekera, 1995.** The velocity gradients normal to the outlet surface are assumed to be zero.

-Wall boundary

Wall functions are special formula for evaluating effective exchange coefficient at the wall (Γ_{wall}), **Versteeg, and Malalasekera,1995**, summarized the expressions for wall function for different dependent variables based on dimensionless quantities;

$$y^+ = \frac{\rho \kappa^{1/2} C_D^{1/4} \delta}{\mu_l} \quad (17)$$

$$u^+ = \frac{1}{\kappa} L_n(E.y^+) \quad (18)$$

Where (δ) is the distance to the wall from the nearby grid node. The constants (κ and E) can be obtained from the law of wall. Usually (K= 0.4107) and (E= 9.793) for smooth wall, **Moult,and Srivatsa, 1977**. In a region very close to the wall, kinetic energy of turbulence is set equal to zero. The value of (ε) is fixed at the near wall point with;

$$\varepsilon = \frac{C_\mu^{3/4}.k^{3/2}}{\kappa.\delta} \quad (19)$$

-Moving boundary

For viscous flow, velocity components normal to the moving boundary (Rotating cylinder) are set to zero while velocity components parallel to the moving boundary are specified as follows:

$$\vec{V} = \omega.r \quad (20)$$

3. NUMERICAL SOLUTION

Computational Fluid Dynamics, commonly known as CFD has becomes an important tool used for the design and analysis of thermal-fluid systems over the last several decades .Increases in computing power have permitted more detailed calculations to be undertaken in significantly less time leading to an expanded envelope for computational modeling. Ultimately, it is desirable to continue the development of newer and more accurate CFD algorithms while benchmarking current computational packages. A detailed summary of the CFD methodology and techniques employed during this study will be discussed in the following sections.

3.1 GAMBIT Software

Geometry and Mesh Building Intelligent Tolls (GAMBIT v2.4.6) mesh generation software is discretizing software used to mesh the turbine blade model. The control volumes in this analysis represent the flow domain on the airfoil with steps and front rotating cylinder. Discretization is the process of subdividing the surfaces that represent the fluid flow and solid regions into smaller areas called cells. In CFD, flow variables are solved from one of the cell to the next until the solution for the entire control volume is completed.

3.2 Geometry Definition

The geometry nodes was built by the developing a computer program to the airfoil equations in the Microsoft Excel program by using the equations of the airfoil boundaries for upper and lower parts and making several modifications to give the exact locations and dimensions of the steps that will be studied.

The testing airfoil and domain was built by the Gambit software with the domain dimensions 3c in from the airfoil original point which is at the leading edge and 4c back word of the airfoil trialing edge and 3c for both upper and lower surfaces of airfoil. The airfoil NACA 0012 cord length was 1m, the front rotating cylinder diameter was (0.1c) and the gap between the cylinder and the airfoil was 1mm.

By importing the vertices of the airfoil coordinates in the Gambit program and convert this nodes to surface and subtracting from the domain to mesh the domain according to the Reynold number value and by using the equations (32 to 33) and **Table 2** and **3**.were the mesh cell number calculated.

3.3 Turbulence Model ($k-\omega$)

Many models under the turbulence model ($k-\omega$) can be used in flow field depending on the type of the applications and the associated boundary conditions that work on it. In the present study, according to the boundary conditions which can work on the turbulence model ($k-\omega$), SST model had been built on a baseline model, namely, (BSL Model), which combines the **Wilcox,1993** ($k-\omega$) model near-wall region with the ($k-\varepsilon$) model in the outer part of the boundary layer, **Peng and Eliasson, 2007**.

In simulations of separating aerodynamic flow, indeed, the success reached with the SST model may largely be attributed to the SST assumption inherent in the modeling formulation. The baseline (BSL) model, on the other hand, enables an alleviation of free stream sensitively in the outer edge of the boundary layer due to the combined ($k-\varepsilon$)model. The shear stress transport equation is given by, **Peng and Eliasson, 2007**,as follows:

$$\frac{\partial \rho k}{\partial t}+\frac{\partial(\rho \overline{U_j} k)}{\partial x_j}=\tau_{ij}\frac{\partial \overline{U_i}}{\partial x_j}-C_k f_k \rho k\omega+\frac{\partial}{\partial x_j}\left[\left(\mu+\frac{\mu_t}{\sigma_k}\right)\frac{\partial k}{\partial x_j}\right] \quad (21)$$

$$\frac{\partial \rho \omega}{\partial t}+\frac{\partial(\rho \overline{U_j} \omega)}{\partial x_j}=C_{\omega 1} f_\omega \frac{\omega}{k}\tau_{ij}\frac{\partial \overline{U_i}}{\partial x_j}-C_{\omega 2}\rho\omega^2+\frac{\partial}{\partial x_j}\left[\left(\mu+\frac{\mu_t}{\sigma_\omega}\right)\frac{\partial \omega}{\partial x_j}\right]+C_\omega \frac{\mu_t}{k}\frac{\partial k}{\partial x_j}\frac{\partial \omega}{\partial x_j} \quad (22)$$

The first three terms on the right-hand side of **Eqs. 21** and **22** are subsequently the production term, the dissipation/destruction term and the diffusion term for (k) and(ω), respectively. The last term in the(ω) equation is the cross diffusion term. This term does not exist in the standard $(k-\omega)$ model but appears in the SST model in the outer part of the wall layer.

Where τ_{ij} is the mass-averaged viscous stress tensor defined as:

$\tau_{ij} = -\rho\overline{u_i u_j}$ And can be calculated using the Boussinesq approximation, **Davidson, 2009**:

$$\tau_{ij} = \mu_t\left[\left(\frac{\partial \overline{U_i}}{\partial x_j}+\frac{\partial \overline{U_j}}{\partial x_i}\right)-\frac{2}{3}\frac{\partial \overline{U_k}}{\partial x_k}\delta_{ij}\right]-\frac{2}{3}\delta_{ij}k\rho \quad (23)$$

And turbulent eddy viscosity can be calculated from the equation. **Peng and Eliasson, 2007:**

$$\mu_t = \frac{a_1\rho k}{\max(a_1\omega/f_\mu, SF_2)} \quad (24)$$

The coefficients, f_μ, f_k,and f_ω, appearing in the transport equation are empirical function of the turbulent Reynolds number, $R_t = \mu_t/\mu$, being free of any wall parameters. These empirical functions take the following forms, **Peng. and Eliasson, 2007**.

$$f_\mu = 0.025 + \left\{1-\exp\left[-\left(\frac{R_t}{10}\right)^{3/4}\right]\right\}\left\{0.975+\frac{0.001}{R_t}\exp\left[-\left(\frac{R_t}{200}\right)^2\right]\right\} \quad (25)$$

$$f_k = 1 - 0.722\exp\left[-\left(\frac{R_t}{10}\right)^4\right] \quad (26)$$

$$f_\omega = 1 + 4.3\exp\left[-\left(\frac{R_t}{1.5}\right)^{1/2}\right] \quad (27)$$

And thus:

$$F_2 = \tanh\left\{\left[\max\left(\frac{2\sqrt{k}}{C_k\omega y}, \frac{500\mu}{\rho\omega y^2}\right)\right]^2\right\} \quad (28)$$

The model constants are **Jones,and Clark,2005** :

Table1. Constants used in the $(k-\omega)$ equation.

C_k	$C_{\omega1}$	$C_{\omega2}$	C_ω	σ_k	σ_ω	a_1
0.09	0.42	0.075	0.75	0.8	1.35	0.31

The general form of the $(k-\omega)$ equation, **Fluent** is:

$$\frac{\partial}{\partial t}(\rho k)+\frac{\partial}{\partial x_i}\left(\rho k\bar{U}_j\right)=G_k+Y_k+\frac{\partial}{\partial x_j}\left(\Gamma_k\ \frac{\partial k}{\partial x_j}\right)+S_k \tag{29}$$

$$\frac{\partial}{\partial t}(\rho \omega)+\frac{\partial}{\partial x_i}\left(\rho \omega\bar{U}_j\right)=G_\omega+Y_\omega+\frac{\partial}{\partial x_j}\left(\Gamma_\omega\ \frac{\partial \omega}{\partial x_j}\right)+D_\omega+S_\omega \tag{30}$$

Where: G_k ,G_ω, Y_k , Y_ω, S_k ,S_ω , and D_ω represent, the generation of (k), generation of (ω), dissipation of (k), dissipation of (ω), source term of (k), source term of (ω) and the cross-diffusion term, respectively.

3.4 Mesh Generation

Standard CFD methods require a mesh that fits the boundaries of the computational domain. The generation of computational mesh that is suitable for the discretized solution of two dimensional Navier-Stokes equations has always been the subject of intensive researches. This kind of problem covers a wide range of engineering applications.

For a complex geometry, the generation of such a mesh is time consuming and often requires modifications to the model geometry. There are mainly two types of approaches in surface meshing, structured and unstructured meshing.

In structured mesh, the governing equations are transformed into the curvilinear coordinate system aligned with the surface. It is trivial for simple shapes, **Hanaa 2006 and Nbras, 2009**. However, it becomes extremely inefficient and time consuming for complex geometries. Therefore, it has been excluded in this study. In the unstructured approach, the integral form of governing equations is discretized and either a finite-volume or finite-element scheme is used. The information regarding the grid is directly incorporated into the discretization. Unstructured grids are in general successful for complex geometries, so it was used in present work.

3.5 Quality of Mesh

It is important to investigate mesh quality and check elements orientation. The importance of quality parameter is the face alignment; it is the parameter that calculates skew-ness of cells. Elements with high skew-ness should be avoided. The face skew-ness can be calculated as:

$$\text{Face skewness} = 1-\frac{\text{length of shorted face diagonal}}{\text{length of longer face diagonal}} \tag{31}$$

This value is in the range of (0.2 to 0.5), FLUENT.

3.6 Grid Independent Test

The way of checking whether the solution is grid independent or not is to create a grid with more cells to compare the solutions of the two models. Grid refinement tests for drag coefficient indicated that a grad size of approximately (100,000 cell) provide sufficient accuracy and resolution to be adopted as the standard for airfoil surface. **Fig.1** shows the grid independency test performed for airfoil surface with steps and rotating cylinder.

3.7 Mesh Smoothness

The number of cells should be more near the viscosity affected regions like walls and smaller at non critical regions. Since the critical part of our domain is the region of airfoil near rotating cylinder surface, a finer mesh is generated there. But, how far the mesh should be refined near the wall prior to extract any result is depend on the value of y^+ near the surface and must be checked. It gives a measure of mesh resolution near the wall boundaries.

It has been shown in **Fig.2** that the averaged value of $y^+$for the surface is less than 100 which is within the range of (SSTk − ω) turbulence model, Jones, and Clark, 2005.

3.8 Total Cell Count

The final point in a good mesh is the total number of cells generated. It is vital to have enough number of cells for a good resolution but memory requirements increase as the number of cells increase. For the present study, an average of (100,000) cell is used. **Fig.3** shown the mesh on the airfoil surfaces

The procedures for calculation the number of the nodes and discretization of the airfoil and flow domain following (Gambit 2.4.6) are:

Refinement Factor: Coarse, medium, and fine mesh types are available. Mesh density varies based upon the assigned refinement factor. The refinement factor values for the mesh densities are given in **Table 2**.

Table 2. Refinement factors.

Mesh density	Refinement factor
Fine	1
Medium	1.5
Coarse	2.25

Using the refinement factor, first cell height is calculated with the following formula, **Gambit 2.4.6:**

$$\text{First Cell Height} = \text{Refinement factor}\left[\frac{\text{Yplus} \times (\text{Characteristic Length}^{0.125} \times \text{Viscosity}^{0.875})}{0.199 \times \text{Velocity}^{0.875} \times \text{Density}^{0.875}}\right] \quad (32)$$

Reynolds number based upon chord length is used to determine Yplus. Yplus values for turbulent flow conditions are summarized in **Table 3**.

Table 3. Flow regime vs. Reynolds number.

Reynolds number	Flow regime	Yplus/Firstcell height
Re≤50000	Turbulent, enhanced wall treatment	Yplus < 10
Re>50000	Turbulent, standard wall functions	Yplus > 30

The number of intervals along each edge is determined by using geometric progression and the following equation, **Gambit 2.4.6.**

$$\text{Intervals} = \text{INT}\left[\frac{\text{Log}\left\{\frac{\text{Edge\_length} \times (\text{Growth ratio} - 1)}{\text{First Cell Height}} + 1.0\right\}}{\text{Log}(\text{Growth ratio})}\right] \quad (33)$$

The edges are meshed using the first cell height and the calculated number of intervals. The entire domain is meshed using a map scheme.

4. METHOD OF SOLUTION

The method of analysis involves the numerical solution of flow field equations:
Continuity equation,
Momentum equation and
Transport equation of turbulence.

The solution algorithm implies modified version of SIMPLE method of **Patanakar, 1980**, which is an iterative sequence consists of two major parts: the SIMPLE procedure,

The SIMPLE algorithm developed by **Patanakar, 1980**, involves one predictor step and one corrector step. It links the solution of the momentum equation with the continuity equation through the pressure. This is accomplished by solving the momentum equation using the guessed pressure field or values from the previous iteration for the parameters appearing in the equation. This yields to new velocity fields.

Thus, the velocity field obtained satisfies the momentum equation but in general violates the conservation of mass principle. Hence, a correction is introduced into the velocity and pressure fields, after that the transport equation for turbulent is solved using the new velocity field.

This iteration sequence is repeated until the residual (error) levels fall below pre-determined maximum allowable limits indicating a converged solution has been achieved. The total maximum residual is taken to be (1*10-5).

Changing the angle of attack and Re number, and finding the separation points and stall conditions of the NACA0012, after that select the optimum locations and dimensions (i.e. depth and length of

the step) to improve the pressure gradients and to move the separation points to the back and delaying the stall.

5. RESULTS

Improvement in performance of the conventional symmetrical airfoil, four digits (NACA 0012) with leading edge rotating cylinder and two steps on its upper side is investigated. The rotating cylinder velocity to main stream velocity ratio,($U/U\infty$) in the range of 1,2,3 and 4 and the change in the positions (0.1c,0.2c,0.3c,0.4c,0.5c) and (0.5c,0.6c,0.7c,0.8c) for first step and second steps respectively, were considered, while, the steps depth and length were kept constant, **Finaish & Stephen 1998.** Assessment of airfoil performance was tested for Reynolds number of 700,000 based on the cord length (c).The numerical results will discuss as follow:-

Fig.5 shows the airfoil lift to drag coefficients ratio for velocity ratio of ($U/U\infty=1$). The flow separation occurs at relatively high angle of attack. The upper surface flow remains attached to the airfoil up to a distance downstream of the leading edge then at it separates and leads to a large separation bubble, with reattached towards the trailing edge. The rotation of the leading edge cylinder results in increased suction over the nose and the smoothness of the transition from the cylinder to the airfoil surface. The same trend was obtained by **Modi, and Mokhtarian, 1988**. The maximum value of the aerodynamic characteristic ratio (lift/drag) reaches up to 34 for the airfoil with steps position at (0.5c and 0.8c).

From **Fig.6** illustrates the increases in momentum injection into the boundary layer as velocity of rotation increase ($U/U\infty=4$) and, delays the flow separation (stall) from the upper airfoil surface and consequently, resulting in a high (Cl_{max}). Different flow patterns can be recognized. It was also noticed that the existence of critical speed is also evident beyond which momentum injection through a moving surface appears to have relatively less effects and the maximum value of the aerodynamic characteristics ratio reach to 38 for the airfoil with steps position at (0.5 and 0.8) at($U/U\infty=2$).

The aerodynamic characteristic ratio (lift/drag) slightly increases between the angle of attack (11^o up to 15^o) as shown in the **Fig.7** for the steps positions at 0.5 c and 0.8 c. For the velocity ration ($U/U\infty=3$) a considerable increases was observed for the same flow conditions (Re=700,000 and $\alpha=15$) and reaches up to 43.

A significant increases in the ratio of lift/drag for combined effect of step positions and velocities ratio, ($U/U\infty=4$) was observed as shown in **Fig.8.** They cause to delay the separation and increase in lift/drag ratio. The maximum ratio was found at the airfoil with the step position at 0.5c and 0.8c which reached up to 47. The flow developments on the upper side of this airfoil configuration were expected. The separation of the airfoil trailing edge and of a primary vortex that separates from the step leading edge induced a secondary vortex in the vicinity of the step. During events of the flow development, these induced vortices may interact with each other in a complicated manner; comprise flow reattachments over the airfoil surface. These flow developments produce large change in the overall lift and drag coefficients.

Fig.9 shows an increase in the lift coefficient with increasing angle of attack for unconventional airfoil due to the effect of the rotating cylinder and steps position compared with normal airfoil, NACA 0012. Also, an increase of 31% in lift coefficient for unconventional airfoil with optimum configuration is obtained when compared with normal airfoil. A same trend for lift coefficient is obtained with the normal airfoil lift coefficient as shown in **Figs.9, 10 and 11**.

A decrease in drag coefficient is noticed for all values of the velocities ratios as the angle of attack are increasing. A reduction of 26% in drag coefficient for unconventional airfoil with optimum configuration is obtained when compared with normal airfoil at the same angle of attack.as shown in **Fig.10.** The trend of drag coefficient for unconventional airfoil is similar to drag coefficient.

The optimum configuration for the unconventional airfoil is found to be at velocities ratio (U/U∞=4) with the steps position at 0.5c and 0.8c as shown in **Fig.11**. A high ratio of lift to drag was observed compared with the same airfoil without leading edge rotating cylinder and steps on the its upper side.

6. CONCLUSIONS

- The rotating cylinder considered to be the best and effective flow control device which was controlling the stall of airfoil flow. The large separation region on stalled airfoil can be reduced significantly by using the rotating cylinder and two upper steps.
- The stalled airfoil flow is sensitive to rotating cylinder speed ratio (U/U∞).
- The lift coefficient of the airfoil is also increased with increase of angle of the attack.
- The rotating cylinder and upper steps causes a decrease in drag and more increase in lift.
- Lift to drag coefficient values of 34,38,43 and 47 are obtained for velocity ratios (U/U∞) 1,2,3 and 4 respectively
- The optimum configuration for the unconventional airfoil is found to be at velocities ratio (U/U∞=4) with the steps positions at 0.5c and 0.8c for best airfoil performance.
- Normal airfoil separates at angle of attack 12^o, while unconventional airfoil with optimum configuration separates at angle of attack 15^o.
- An increase of 31% in lift coefficient for unconventional airfoil with optimum configuration is obtained compared with normal airfoil.
- A reduction of 26% in drag coefficient for unconventional airfoil with optimum configuration is obtained compared with normal airfoil at the same angle of attack.

NOMENCLATURE:

C : cord (m)

CL: lift coefficient

DL: drag coefficient

P: pressure (N/m^2)

Re: Reynolds number

U∞: uniform flow velocity (m/s)

Uc: velocity of the rotational cylinder (m/s)

α: angle of attack (Degree)

μ: viscosity (kg/m.s)

u_i, u_j: velocity in tenser notation (m/s)

x_i: position vector in tensor notation (m)

δ_{ij}: Kronecker delta

ρ: density (kg/m^3)

τ_{ij}: shear stress (N/m^2)

REFERENCES

- Al- Tornachi, S.J. and Abu- Tabikh, M.I., 1998, *Computation of the Flow Around Airfoils and Wings under High Lift Separated Flow Condition*, Dept. of Mechanical Engineer, University of Technology, Iraq, Journal Eng & technology Vol. 17, No.9.

- Al-Garni, A. Z.,Al-Garni,AM; Ahmed, SA; Sahin, AZ. 2000, *Flow Control for an Airfoil with Leading-Edge Rotation: an Experimental Study*, AMER INST AERONAUT ASTRONAUT, JORNAL OF AIRCRAFT; pp: 617-622; Vol: 37.

- Buckholtz, R.H.,1986, *The Functional Role of Wing Corrugations in Living System*, Department of Mechanical Engineering, Columbia University, New Yourk, NY 10027.

- Cichy, D. R., Harris, J. W., and MacKay, J. K., 1972, *Flight Tests of a Rotating Cylinder Flap on a North American Rockwell Yov-10A Aircraft*, NASA CR-2135.

- Davidson, L., 2009, *An Introduction To Turbulence Models*, http://www.tfd.chalmers.se, 16.

- Fathi Finaish and Stephen Witherspoon., 1998, *Aerodynamic Performance of an Airfoil with Step-induced Vortex for Lift Augmentation.* Dept. of Mechanical and Aerospace, University of Missouri, Rolla, MO 65401.

- Favre, A., 1938, *Contribution of an Experimental Studies of Three-dimensional Hydrodynamic*, Ph.D Thesis presented to the University of Paris.

- Ferziger, J. H. and Peric, M., 1999, *Computational Methods for Fluid Dynamics*, 2nd Edition Springer, Berlin.

- Freymuth, P., Jackson, S., and Bank, W., 1989, *Toward Dynamic Separation without Dynamic Stall*. Dept. of Aerospace Engineering Sciences, University of Colorado, Boulder, CO 80309, USA. Experiments in Fluids. Springer-Verlag,

- Hanaa, A. H., 2006, *Numerical and Experimental Investigation on the Effect of Restriction Shape on Characteristics of Airflow in a Square Duct*, Ph.D. thesis, Mech. Eng. Dept., Univ. of Technology.

- Jones, D.A., and Clark, D.B., June 2005. *Simulation of a Wing-body Junction Experiment using the Fluent Code*, Commonwealth of Australia AR-013-426.

- Modi, V.J. and Mokhtarian, F., 1988, *Effect of Moving Surfaces on the Airfoil Boundary-Layer Control*, Aircraft J., Vol.27, No.1, pp.42-50,

- Moult, A. and Srivatsa, S. K., 1977, *Kora-2 A Computer Code for Axi-symetrical Combustion Chambers*, Chan computer code 201, London, England.

- Nbras, H., 2009, *Effect of Riblet Geometry on Drag Reduction and its Application on Airfoil*, Ph.D. thesis, Mech. Eng. Dept., Univ. of Technology.

- Patanakar, S. V., 1980, *Numerical Heat Transfer and Fluid Flow*, Series in computational methods in mechanics and thermal sciences. Hemisphere Publ. Corp., McGraw-Hill.

- Peng, S. H. and Eliasson, P., 2007, *Examination of the Shear Stress Transport Assumption with a Low -Reynolds Number* $(k-\omega)$ *Model for Aerodynamic Flow*, American Institute of Aeronautics and Astronautics.

- Popelka Lukas, Simurda David, Matejka Milan, Souckova Natalie, 2011,*Boundary Layer Transition, Separation and Flow Control on Airfoils and Bodies in CFD, Wind-tunnel and in-Flight Studies*, proceeding of the 27th International Congress of the Aeronautical Sciences, Prague.

- Sahu, R.D. and Patnaik, B.S.V., 2010, *Momentum Injection Control of Flow Past an Aerofoil*, Proceedings of the 37th National & 4th International Conference on Fluid Mechanics and Fluid Power December 16-18, IIT Madras, Chennai, India.

- Versteeg, H. K., and Malalasekera, W., 1995, *An introduction to Computational Fluid Dynamics, the Ffinite Volume Method*, Longman Scientific and technical.

- White, F. W., 1991, *Viscous Fluid Flow, 2nd Ed*., McGraw-Hill, New York.

- Wilcox, D. C., 1993, *Turbulence Modeling for CFD*, DCW Industries Inc., La Canada, California.
- Yeung, W.W.H., 2006. *Lift Enhancement on Unconventional Airfoils*, Journal Mekanikal December, No. 22, 17-25.

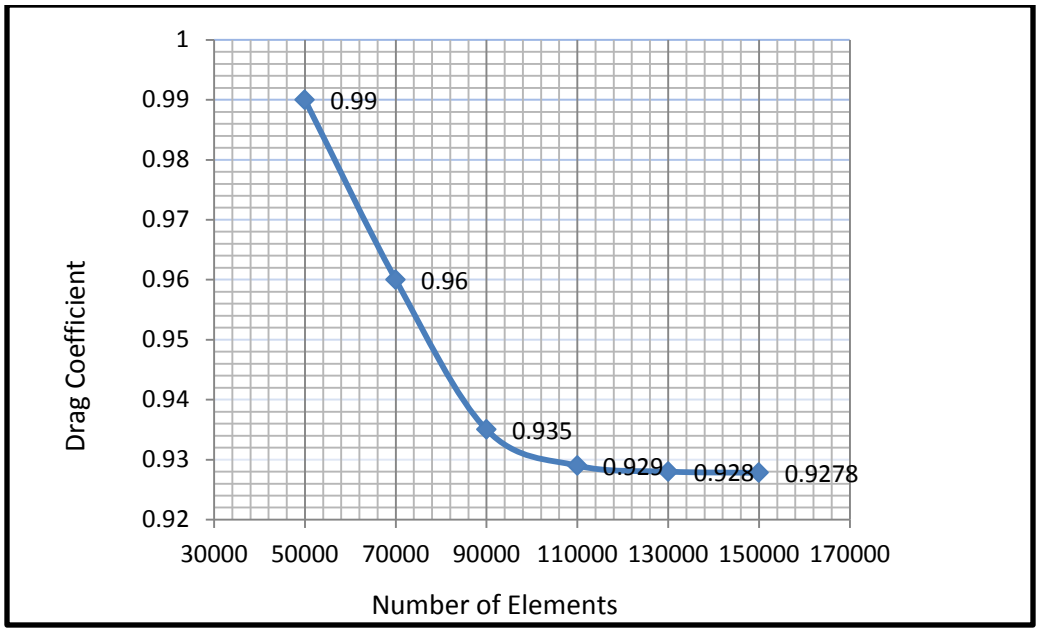

Figure1. Mesh independency test for airfoil with steps and rotating cylinder.

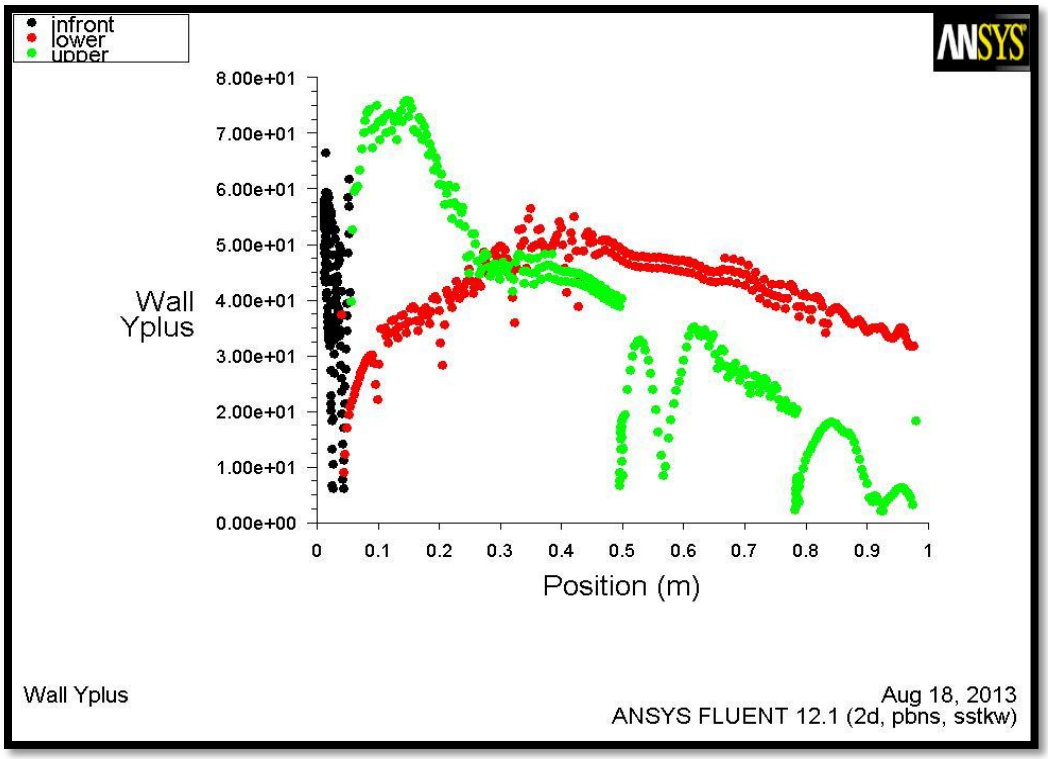

Figure 2. Wall (y^+) variation along the airfoil with steps and rotating cylinder.

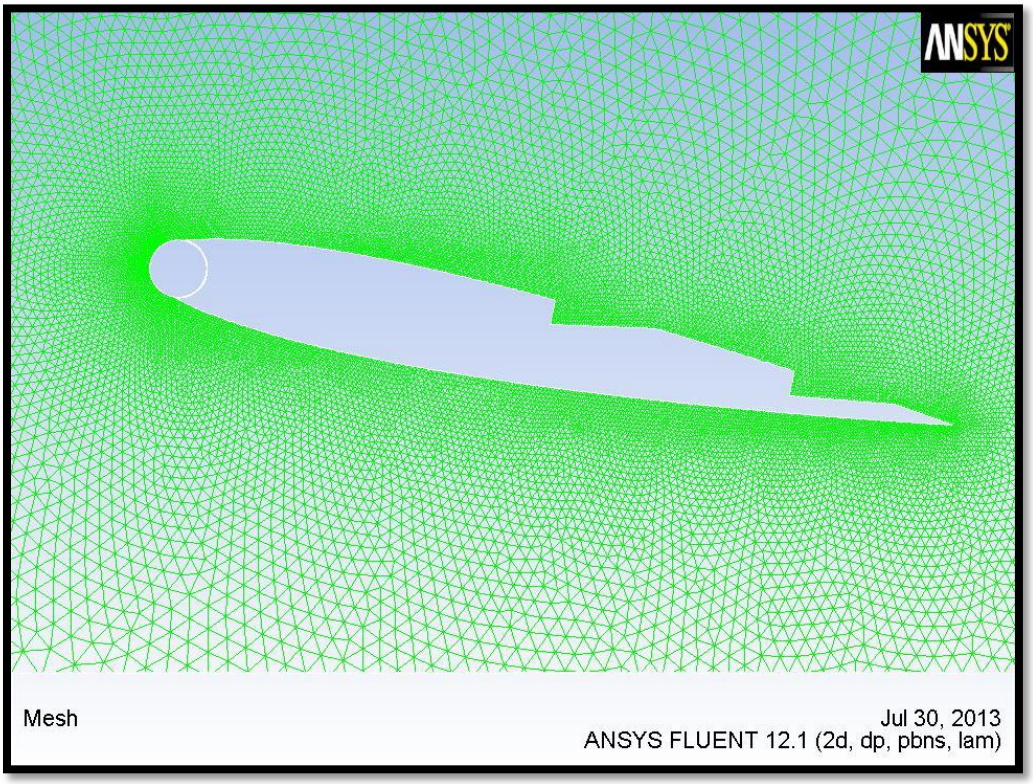

Figure3. Mesh on the airfoil surfaces.

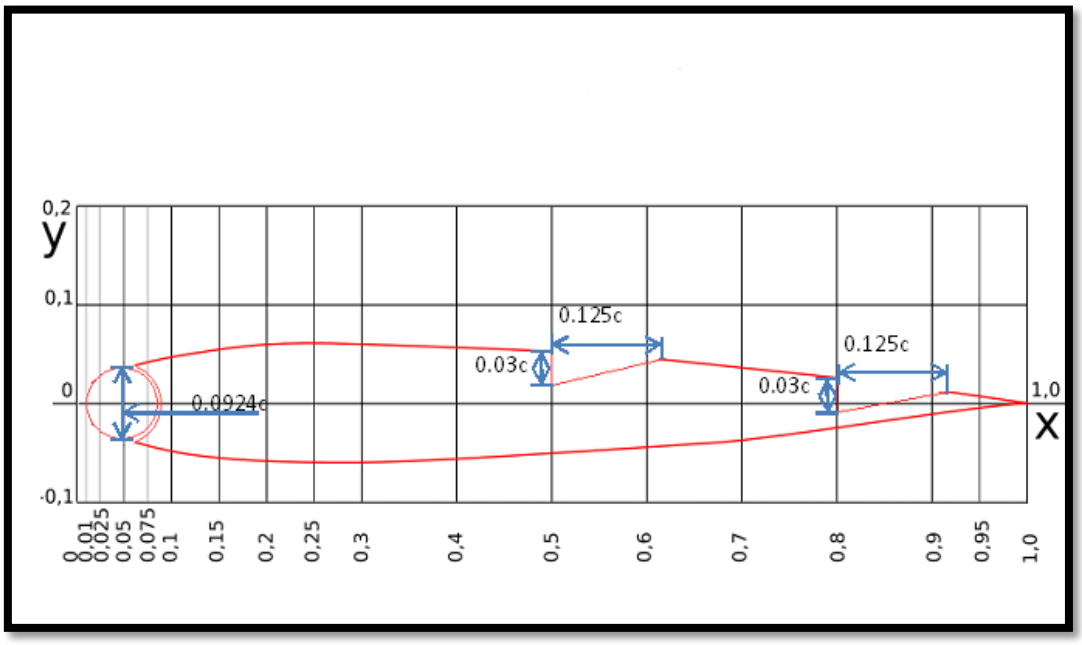

Figure4. Geometry and coordinates of the unconventional airfoil consists of front rotating cylinder and double steps on its upper surface.

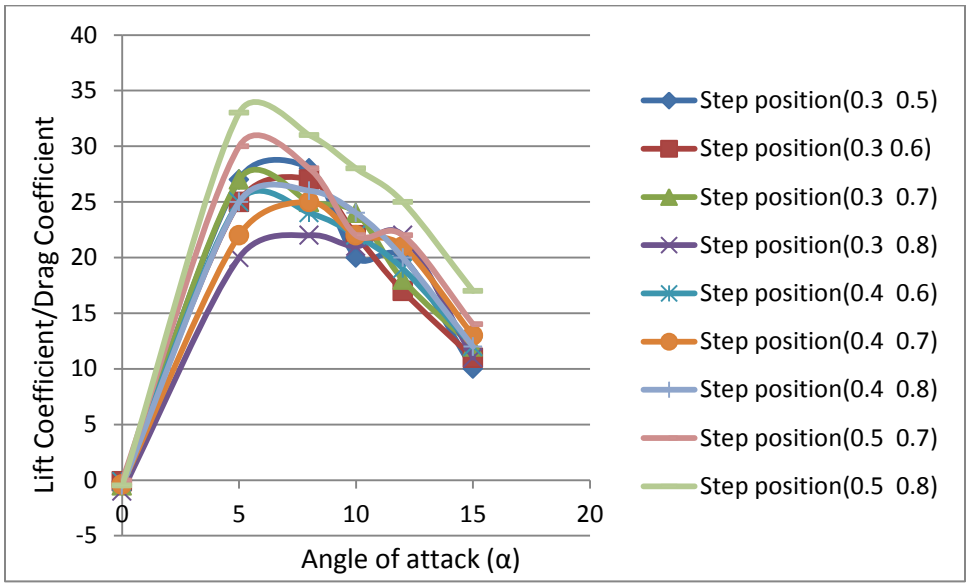

Figure 5. Lift to drag coefficient ratio with various angles of attack (α) at velocity ratio (U/U∞=1).

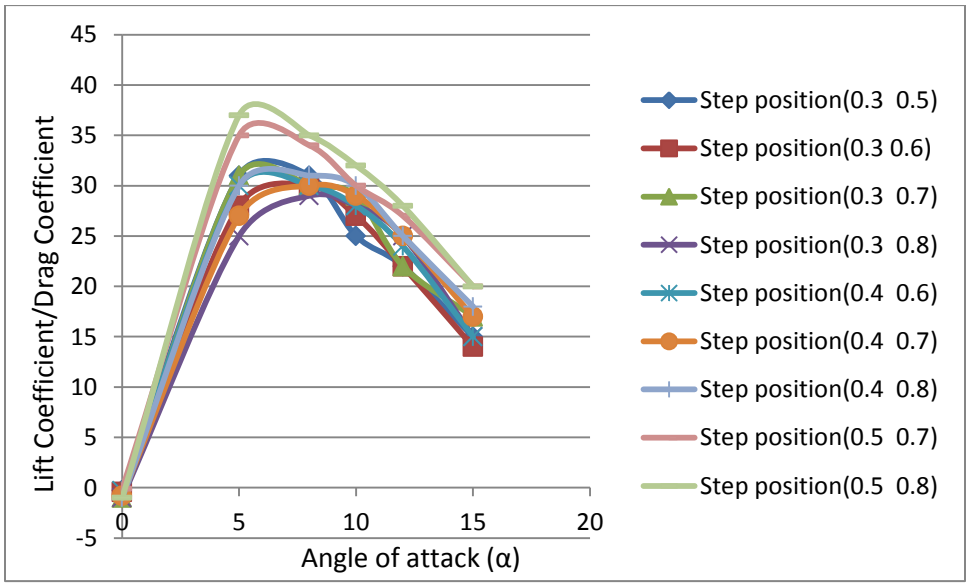

Figure 6. Lift to drag coefficient ratio with various angles of attack (α) at velocity ratio (U/U∞=2).

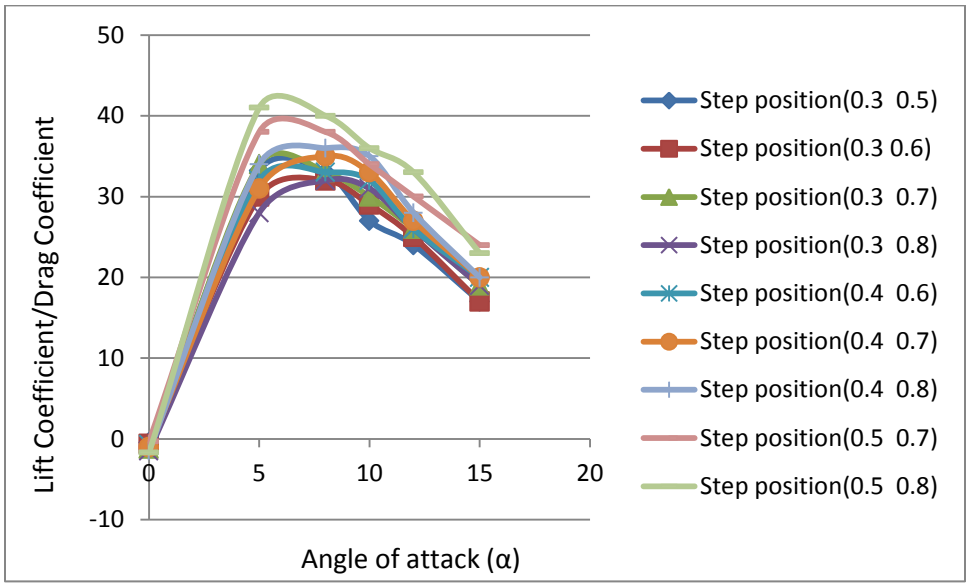

Figure 7. Lift to drag coefficient ratio with various angles of attack (α) at velocity ratio (U/U∞=3).

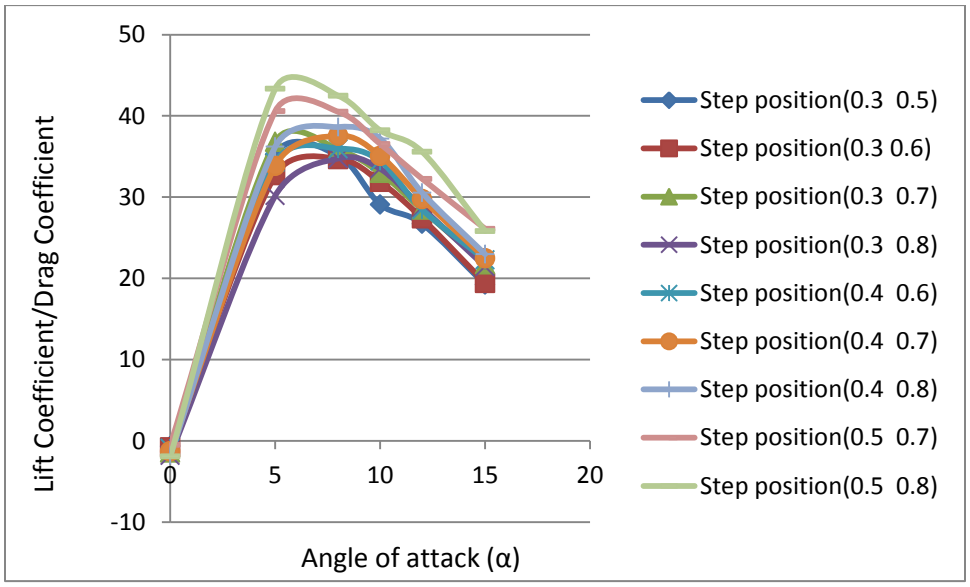

Figure 8. Lift to drag coefficient ratio with various angles of attack (α) at velocity ratio (U/U∞=4).

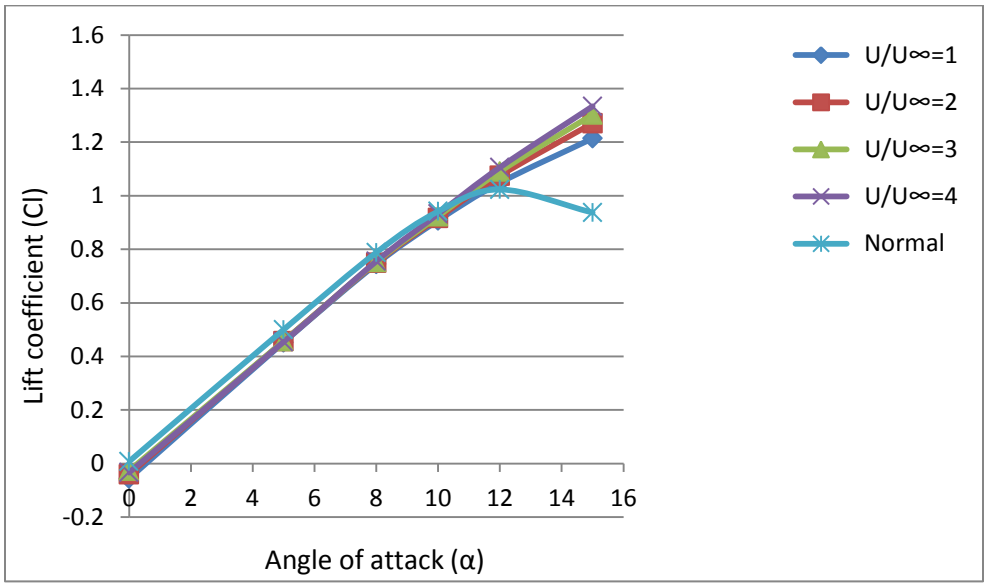

Figure 9. Lift coefficient with various angles of attack at steps positions 0.5c and 0.8c.

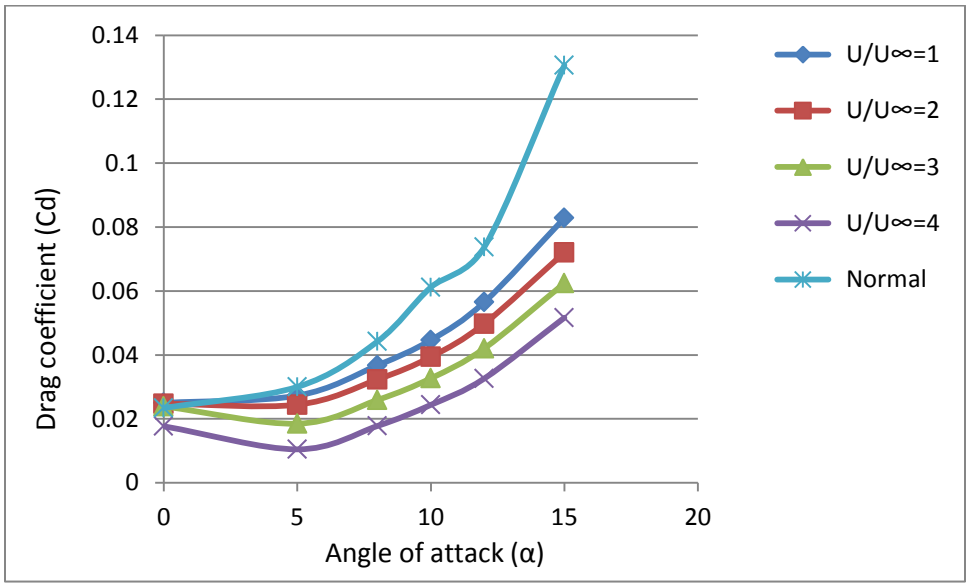

Figure 10. Drag coefficient with various angles of attack at steps positions 0.5c and 0.8c.

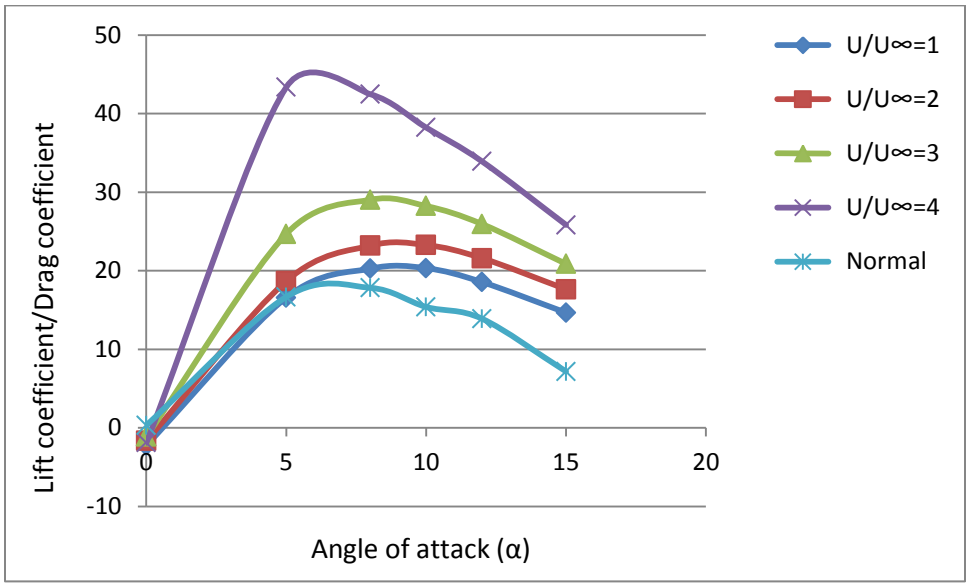

Figure 11. Lift to drag coefficient ratio with various angles of attack for steps positions at 0.5c and 0.8c.